# Supplementary materials for: The risky middle of the road - probabilities of triggering climate tipping points and how they increase due to tipping points within the Earth's carbon cycle

Jakob Deutloff[1, 2, 3], Hermann Held[4], and Timothy M Lenton[1]

[1]Global Systems Institute, University of Exeter, Exeter, UK.
[2]Center for Earth System Research and Sustainability (CEN), Meteorological Institute, Universität Hamburg, Hamburg, Germany.
[3]International Max Planck Research School on Earth System Modelling (IMPRS-ESM), Hamburg, Germany.
[4]Research Unit Sustainability and Global Change and Center for Earth System Research and Sustainability, Universität Hamburg, Germany.

**Correspondence:** Jakob Deutloff (jakob.deutloff@mpimet.mpg.de)

## S1 Timestepping Scheme

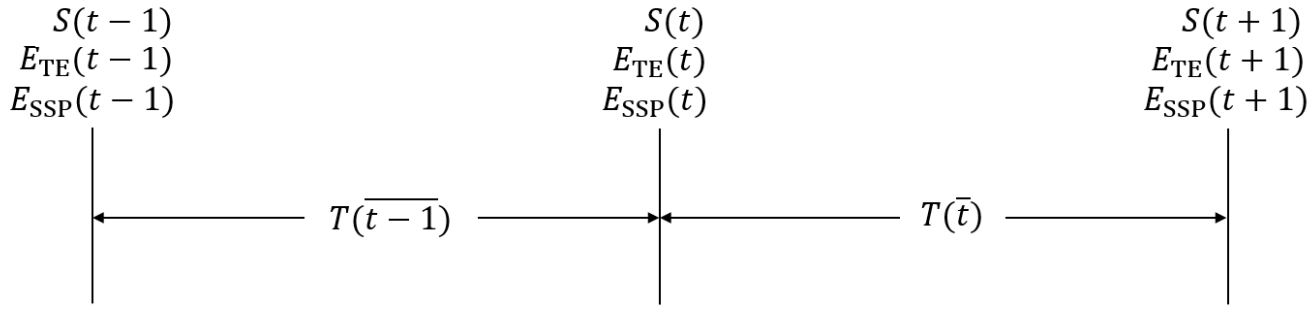


**Figure S1.** Schematic representation of the timestepping scheme in FaIR. Vertical lines represent single timesteps and horizontal arrows the time between them. Variables should be interpreted as single values given at a time step (over vertical lines), or as averages between the timesteps (between vertical lines).

## S2 Derivation of CTEM Formulation

To derive the discrete form of CTEM, we start by rewriting the logistic equation for $S$

$$\frac{dS}{dt} = r\frac{T}{P}S - \frac{rT}{PK}S^2 \tag{1}$$

We simplify this equation by defining $a$ and $b$ as

$$a := r\frac{T}{P} \tag{2}$$

$$b := \frac{rT}{PK}. \tag{3}$$

With those definitions, we can rewrite eq. 1 as

$$\frac{dS}{dt} = aS - bS^2. \tag{4}$$

We further define

$$u := S^{-1}, \tag{5}$$

which gives us

$$S = u^{-1},$$
$$\frac{dS}{du} = -u^{-2}\frac{du}{dt},$$

with which we can rewrite eq. 4 as

$$-u^{-2}\frac{du}{dt} = au^{-1} - bu^{-2}. \tag{6}$$

We multiply eq. 6 with $-u^2$ and rearrange which gives us

$$\frac{du}{dt} + au = b. \tag{7}$$

As eq. 7 is a Bernoulli differential equation, we know that an exact solution exists, which can be derived analytically. Since output variables from FaIR such as $T$ are treated as constant between timesteps, this also holds for $a$ and $b$ which are calculated using eq. 2 and eq, 3 with $T = T(\overline{t-1})$. Hence, eq. 7 is a Bernoulli differential equation with constant coefficients which can be solved with an integrating factor $I$ defined as

$$I := e^{at}.$$

We now multiply eq. 7 with $I$ which yields

$$e^{at}\frac{du}{dt} + e^{at}au = be^{at}.$$

This equation is now integrated from $t-1$ to $t$ to give the new solution for $u$ at $t$

$$\int_{t-1}^{t} e^{at'} \frac{du}{dt'} + e^{at'} au \, dt' = \int_{t-1}^{t} be^{at'} \, dt'.$$

The left-hand integral can now be solved using the chain rule

$$\left[e^{at'} u\right]_{t-1}^{t} = b \int_{t-1}^{t} e^{at'} \, dt'.$$

The right-hand integral can be solved directly, and we derive

$$e^{at} U_2 - e^{a(t-1)} U_1 = \frac{b}{a} \left(e^{at} - e^{a(t-1)}\right).$$

Here, $u$ is a function of $t$ but to prevent confusion of brackets, we write $U_2$ for $u(t)$ and $U_1$ for $u(t-1)$. We simplify this equation by dividing by $e^{at}$ and defining $\Delta t := t - (t-1)$

$$U_2 - e^{-a\Delta t} U_1 = \frac{a}{b} \left(1 - e^{-a\Delta t}\right).$$

Now, we resubstitute for $u$ using eq. 5

$$S_2^{-1} - e^{-a\Delta t} S_1^{-1} = \frac{b}{a} \left(1 - e^{-a\Delta t}\right),$$

which can be rewritten as

$$S_2 = \left(e^{-a\Delta t} \left(S_1^{-1} - \frac{b}{a}\right) + \frac{b}{a}\right)^{-1}.$$

Explicitly showing the time dependency of $S$, $b$ and $a$, we derive

$$S(t) = \left(e^{-a(\overline{t-1})\Delta t} \left(S^{-1}(t-1) - \frac{b(\overline{t-1})}{a(\overline{t-1})}\right) + \frac{b(\overline{t-1})}{a(\overline{t-1})}\right)^{-1}.$$

Bars over $t$ denote that the respective variable is treated as the average value between two gridpoints, whereas variables without a bar over $t$ are defined at the gridpoints (Fig. S1).

## S3 Calibration of CTEM

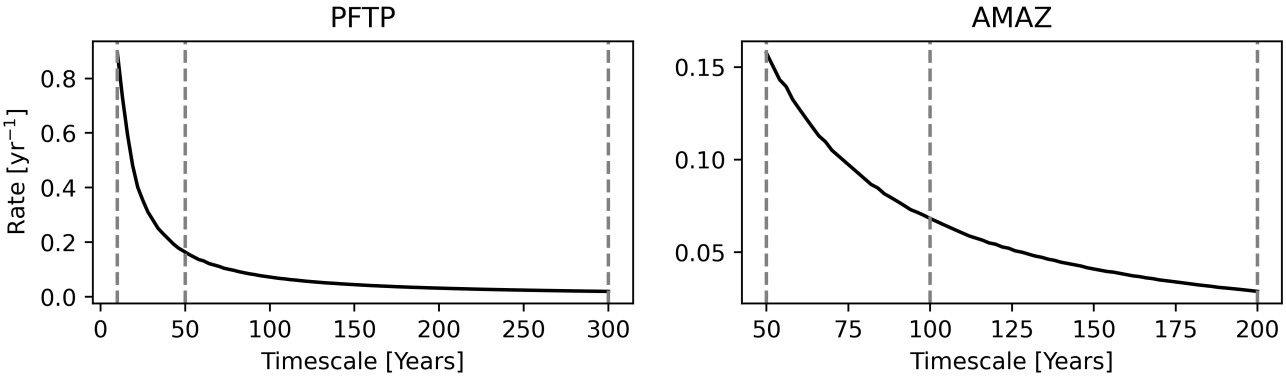


**Figure S2.** Calibrated rate ($r$) for $H$ of PFTP and AMAZ. Grey vertical lines denote maximum, mean and minimum estimate of $H$ from Tab. 1.

For the definition of $S_0$, we define the tipping timescale as the period over which 99% of the cumulative carbon emissions occur, which means $S_0$ is defined as 0.5% of $K$ ($K_{\max}$ for PFAT). All calibrations of $r$ are performed under the SSP5-8.5 scenario, as most model studies which inform the emission estimates of all three TEs were performed under the corresponding RCP8.5 scenario (Armstrong McKay et al., 2022). To increase transparency, all TEs are calibrated individually, with the other two TEs being deactivated. Furthermore, we use the default parameterization of FaIR for all calibrations.

For the calibration of PFTP and AMAZ, we use the respective mean estimate for $P$ and $K$. We calibrate $r$ by splitting the respective range of $H$ from Tab. 1 into $\sim 100$ equally spaced bins, with one value of $r$ fitted to each bin. We define the following objective function, which resembles the squared difference ($D$) between the observed $H$ of the model and the expected value:

$$D = ((Y_{\mathrm{end}} - Y_{\mathrm{start}}) - H)^2, \tag{8}$$

with $Y_{\mathrm{end}}$ being the year in which 99.5% of maximum cumulative emissions are emitted and $Y_{\mathrm{start}}$ the year in which the respective TE is triggered. These values are looked up in the model results without any further time-aggregation being necessary, which increases the performance of the calibration algorithm. The objective function is minimized for each bin of $H$ for AMAZ and PFTP using the Nealder-Mead algorithm (Gao and Han, 2012), which gives the calibrated values of $r$ (Fig. S2). The objective function has been successfully minimized to zero for all bins of $H$ for PFTP and AMAZ.

For PFAT, we only calibrate $r$ for the mean estimate of $H$, using the mean values of $P$ and $K_{\max}$ with $K = K_{\max}$ at all times. This is due to the fact that the timescale over which the emissions from PFAT occur is already included in the ranges of $F_{100}$ and $F_{300}$. The value of $r = 0.041\ \mathrm{yr}^{-1}$ corresponding to the mean value of $H = 200\ \mathrm{years}$ is determined by using the objective function (eq. 8), which is minimized to zero.

## S4 Test of CTEM Calibration

Here, we investigate how well the calibrated version of CTEM resembles the estimated values of $H$ of PFTP, AMAZ and $F_{100}$ and $F_{300}$ of PFAT from Tab. 1.

To test the emission feedbacks in 2100 and 2300 of PFAT, we generate 10 equally spaced values of $F_{100}$ and $F_{300}$, covering the whole uncertainty range and 10 equally spaced values of $P$, also covering the respective uncertainty range. With this parameter set, we generate 100 model runs, one for each combination of pairs of $F_{100}$ and $F_{300}$ and $P$. CTEM is coupled to FaIR which is run with its default parameterization under SSP5-8.5, which has also been used for the calibration of CTEM. Now we calculate the difference between the cumulative carbon emissions from CTEM and the expected cumulative carbon emissions based on the values of $F_{100}$ and $F_{300}$ and $T$ for the years 2100 and 2300. In 2100 there are significant deviations between the two, with the cumulative emissions of PFAT from CTEM being smaller than expected (Fig. S4). The relative error of the cumulative carbon emissions in 2100 increases with increasing values for $P$, whereas the value of $F_{100}$ does not seem to have an effect on the error. Maximum errors of up to 80% are reached for the highest realization of $P$. Nevertheless, the relative error is reduced to values below 5% for all combinations of $F_{300}$ and $P$ in 2300. This implies that the medium $H$ is too large to allow for high enough emissions between crossing the tipping point of PFAT and 2100. However, we regard this as the best possible implementation of PFAT since the long-term cumulative carbon emissions still roughly match the estimates and lower values of $H$ would lead to potentially unrealistic abrupt carbon emissions.

For PFTP and AMAZ, we test how well the estimated values of $H$ are met by CTEM for various combinations of $K$ and $P$. We produce 10 equally spaced values of $K$ and $P$, covering the whole uncertainty range and run the model for each combination for both PFTP and AMAZ, with all other TEs within CTEM being deactivated. In this manner, we produce 100 model runs for the minimum, the mean, and the maximum estimate of $H$ for PFTP and AMAZ. FaIR is again run with its default parameterization under SSP5-8.5. The relative error in $H$ of PFTP and AMAZ increases with increasing values for $H$, with CTEM producing smaller values of $H$ than expected for low $P$ and higher values for high $P$. (Fig. S3). Differences in $K$ seem to have nearly no impact on the error in $H$ for both AMAZ and PFTP. Notably, the relative errors in $H$ are higher for AMAZ, with -27% and 45% being reached for the maximum estimate of $H$. For PFTP, the errors are more symmetric, lying between -19% and 19% for the maximum estimate of $H$. The change of sign of the errors around the mean value of $P$ makes sense, as the mean value of $P$ has been used for the calibration. The observed lower values of $H$ for low $P$ and higher values of $H$ for high $P$ can be explained by the rate-dependence of both TEs, with higher exceedance of $P$ leading to faster tipping. As the increase of $T$ slows down over time under SSP5-8.5 (Fig. S8), lower values of $P$ lead to lower $H$ and vice versa. Hence, the observed errors in $H$ of PFTP and AMAZ from CTEM comply with the rate dependence of both TEs and are therefore regarded to be realistic.

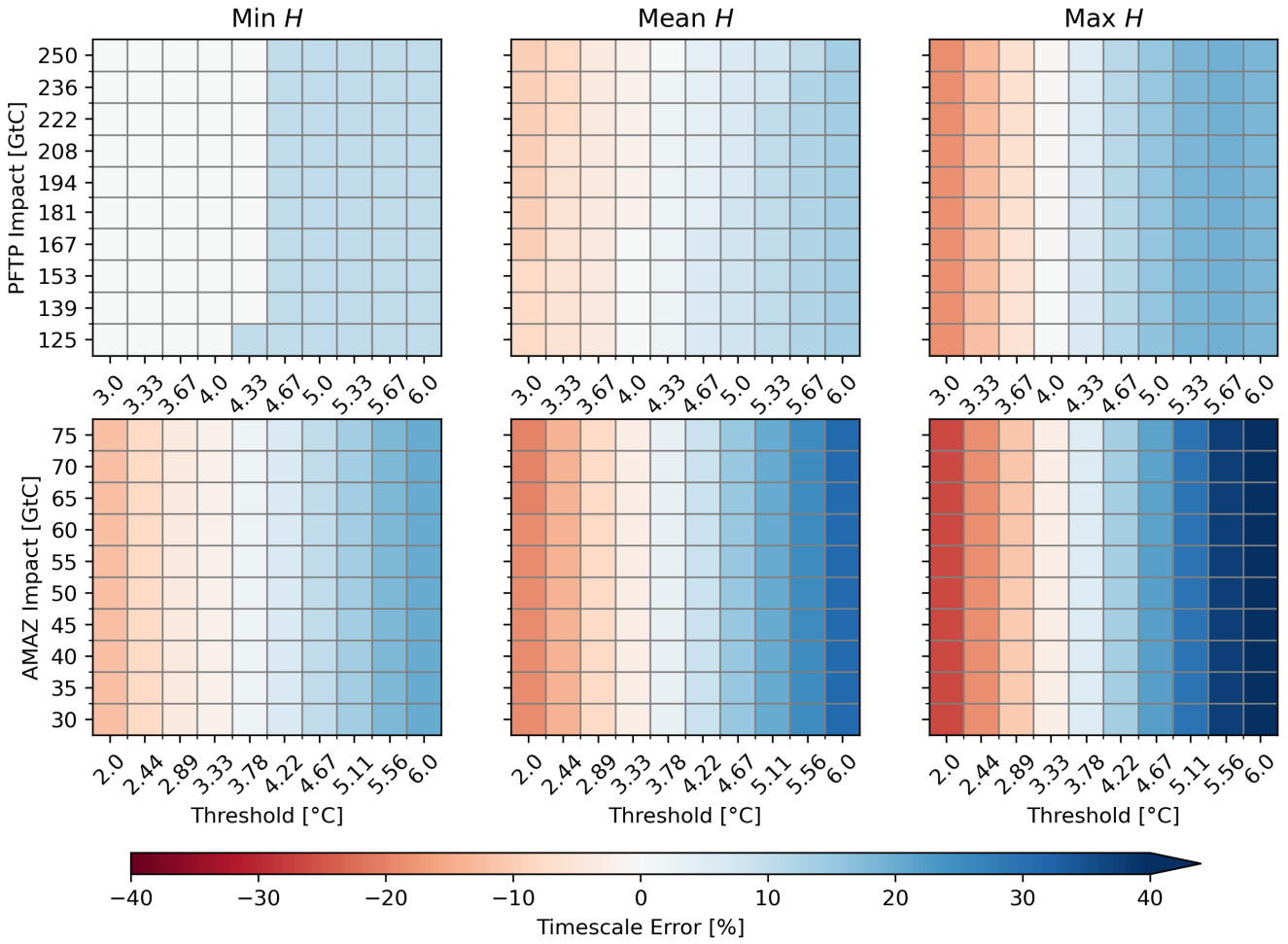


**Figure S3.** Deviations between the expected and the modelled $H$ from CTEM in percent for the minimum, mean, and maximum estimate of $H$ of PFTP and AMAZ with values of $K$ and $P$ equally spaced between the respective maximum and minimum estimate. One box represents one model realization with the respective values of $P$ and $K$ used for PFTP (upper row) or AMAZ (lower row) with all other TEs within CTEM being deactivated and FaIR run with default parametrization under SSP5-8.5.

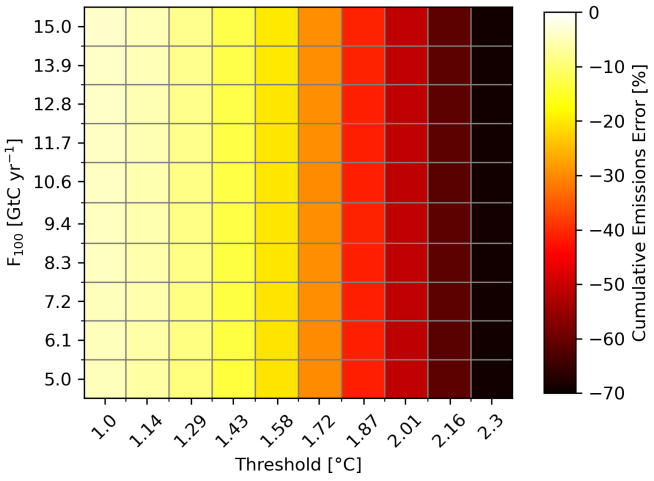


**Figure S4.** Deviations between the expected and the modelled cumulative carbon emissions from PFAT in 2100. One box represents one model realization with the respective values of $P$ and $F_{100}$ used for PFAT, with all other TEs within CTEM being deactivated and FaIR run with default parametrization under SSP5-8.5.

## S5 Probability distributions used in CTEM

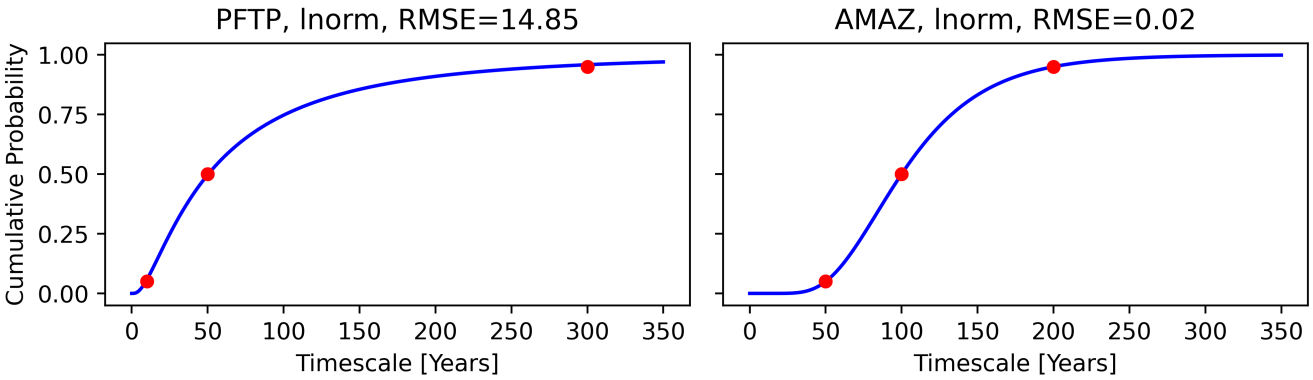


**Figure S5.** Cumulative distribution functions of $H$ for PFTP and AMAZ, together with the RMSE between the given percentiles (red dots) and the actual percentiles of the respective distribution. The title states TE, distribution and RMSE in years.

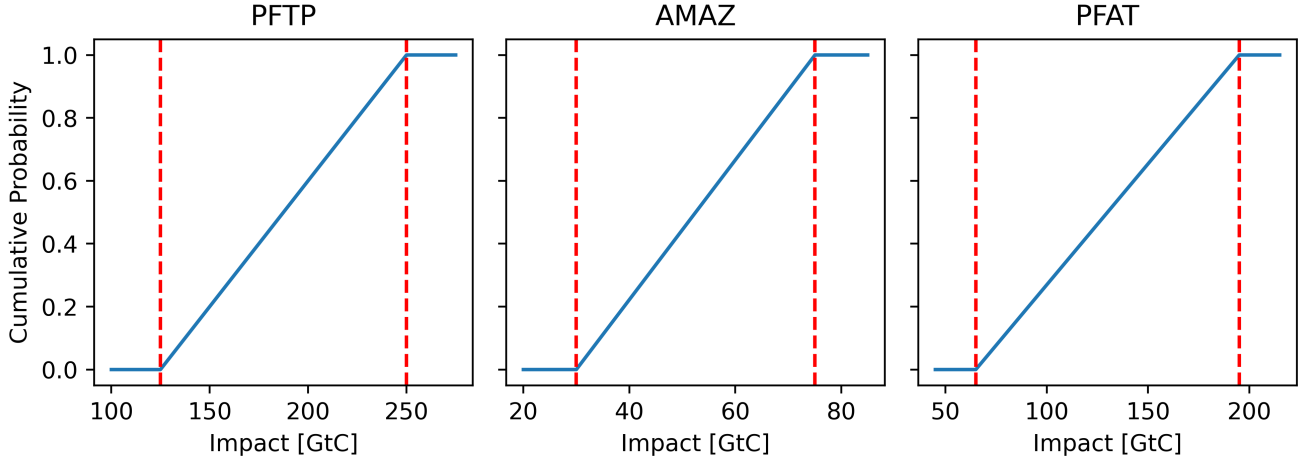


**Figure S6.** Cumulative distribution functions of $K$ for AMAZ and PFTP and $K_{\max}$ for PFAT. The dotted red lines indicate the range of the respective variable from Tab. 1

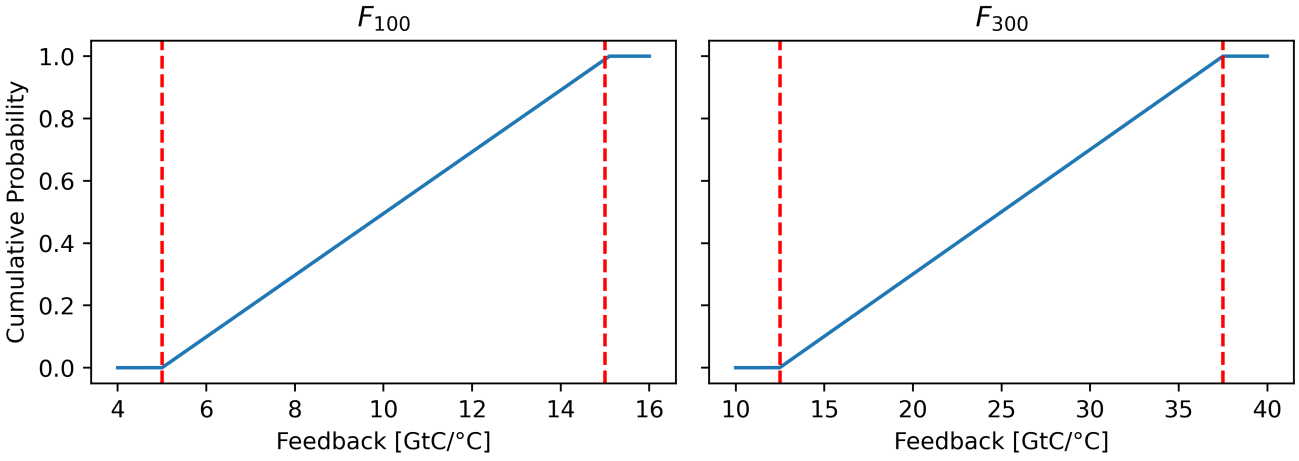


**Figure S7.** Cumulative distribution function of $F_{100}$ and $F_{300}$ of PFAT. The dotted red lines indicate the range of the respective variable from Tab. 1

## S6 Robustness of Ensemble Results

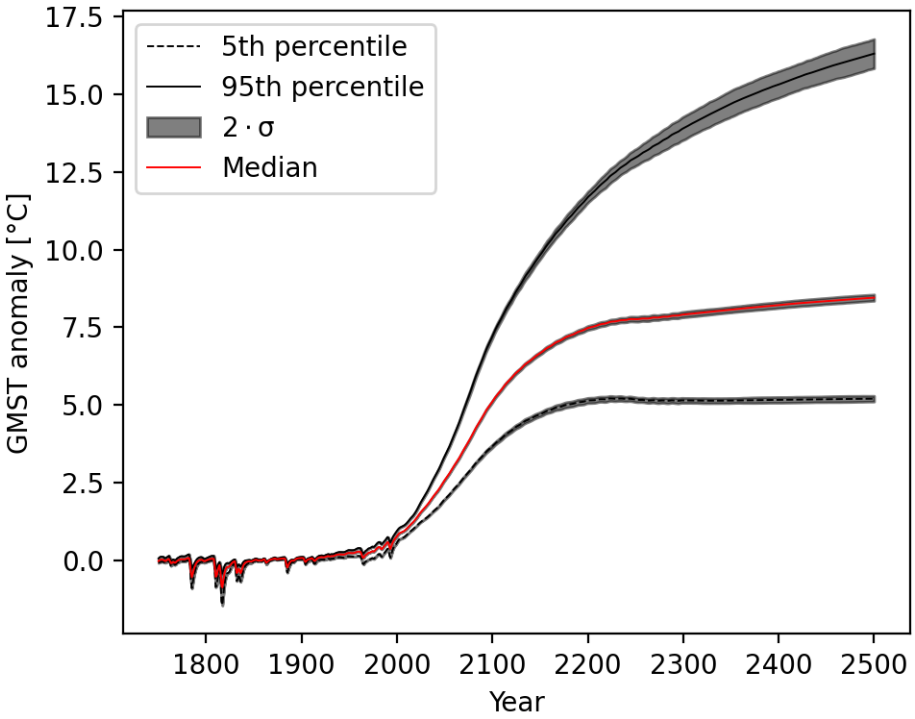


**Figure S8.** Comparison of the 5th percentile, the median and the 95th percentile of $T$ between 20 coupled ensembles with 5000 members each. Mean estimate from all ensembles and two times standard deviation ($\sigma$) between the ensembles.

## S7 Carbon Emissions from Carbon Tipping Elements

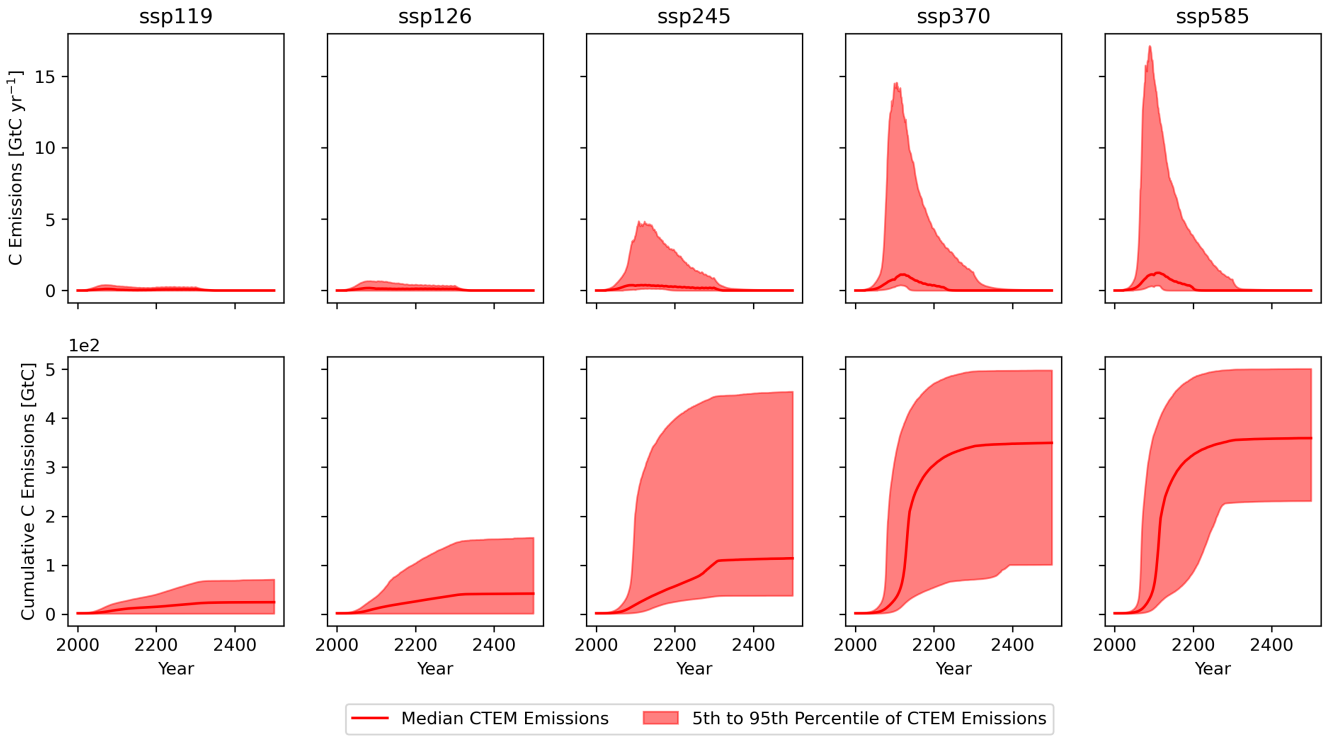


**Figure S9.** Carbon emissions and cumulative carbon emissions from the carbon TEs (modelled by CTEM) between 2000 and 2500.

## S8 Atmospheric Concentrations of Carbon Dioxide and Methane

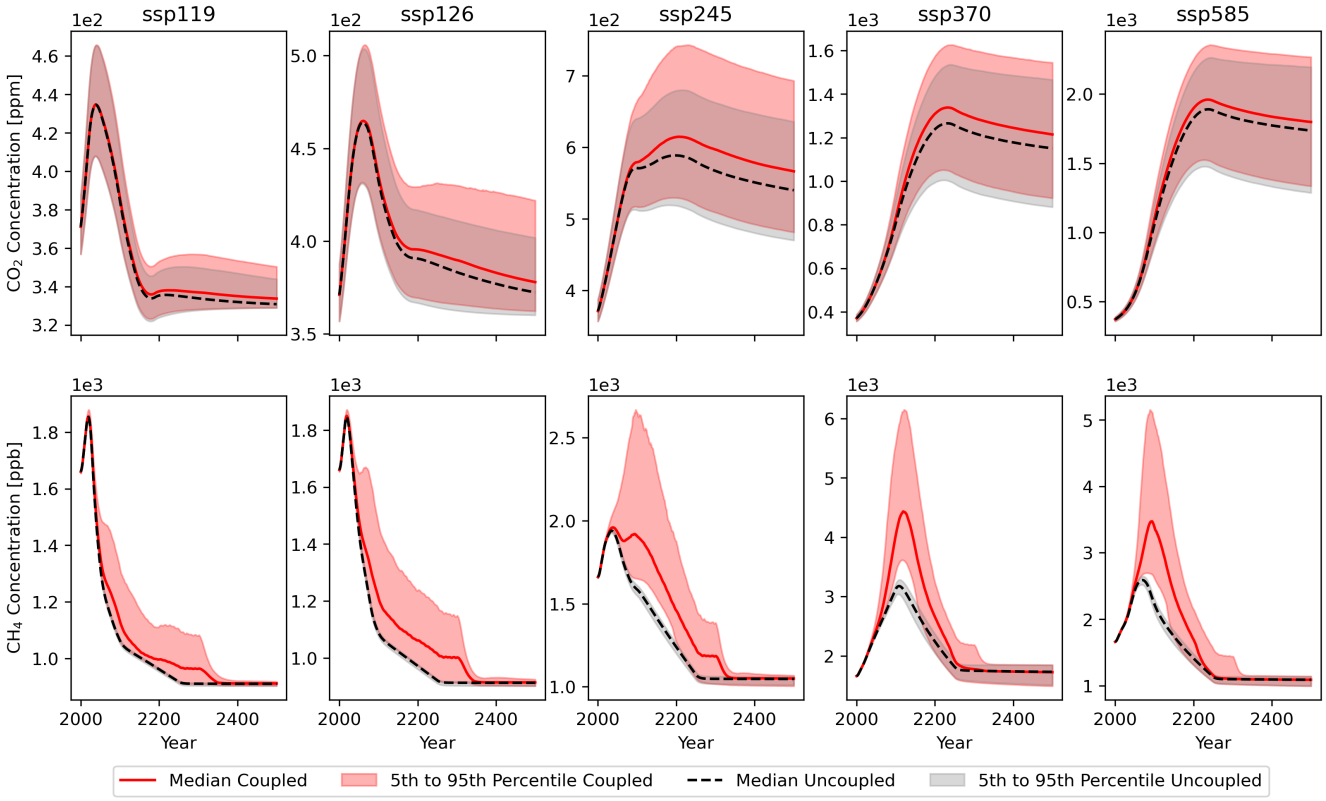


**Figure S10.** Atmospheric concentrations of $CO_2$ and $CH_4$ of the coupled and the uncoupled model ensemble for the Tier1 SSPs.

## S9 Probabilities of Triggering Climate Tipping Elements

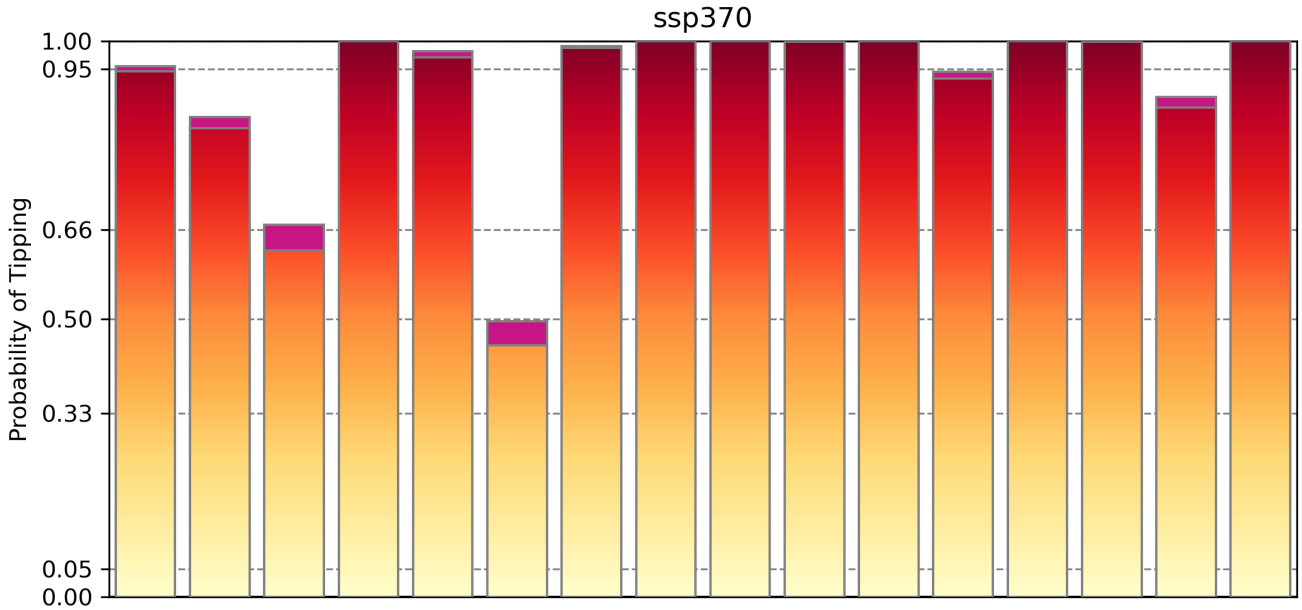


| | | | | | | | | | | | | | | | | |
|---|---|---|---|---|---|---|---|---|---|---|---|---|---|---|---|---|
| 0.5 | 2081 | 2092 | 2175 | 2029 | 2086 | | 2069 | 2042 | 2025 | 2035 | 2025 | 2095 | 2025 | 2064 | 2092 | 2025 |
| 0.5 | 2085 | 2098 | 2222 | 2029 | 2092 | | 2071 | 2043 | 2025 | 2035 | 2025 | 2100 | 2025 | 2065 | 2099 | 2025 |
| 0.95 | 2299 | | | 2042 | 2149 | | 2119 | 2070 | 2072 | 2079 | 2056 | | 2047 | 2095 | | 2055 |
| 0.95 | | | | 2042 | 2185 | | 2132 | 2071 | 2075 | 2082 | 2056 | | 2047 | 2099 | | 2056 |

**Figure S11.** Probabilities of triggering the TEs by 2500 under SSP3-7.0. Additional probabilities from the carbon TEs are marked in purple. The table underneath states the years in which the 50% and 95% probability is crossed, with purple including carbon emissions from carbon TEs and black not.

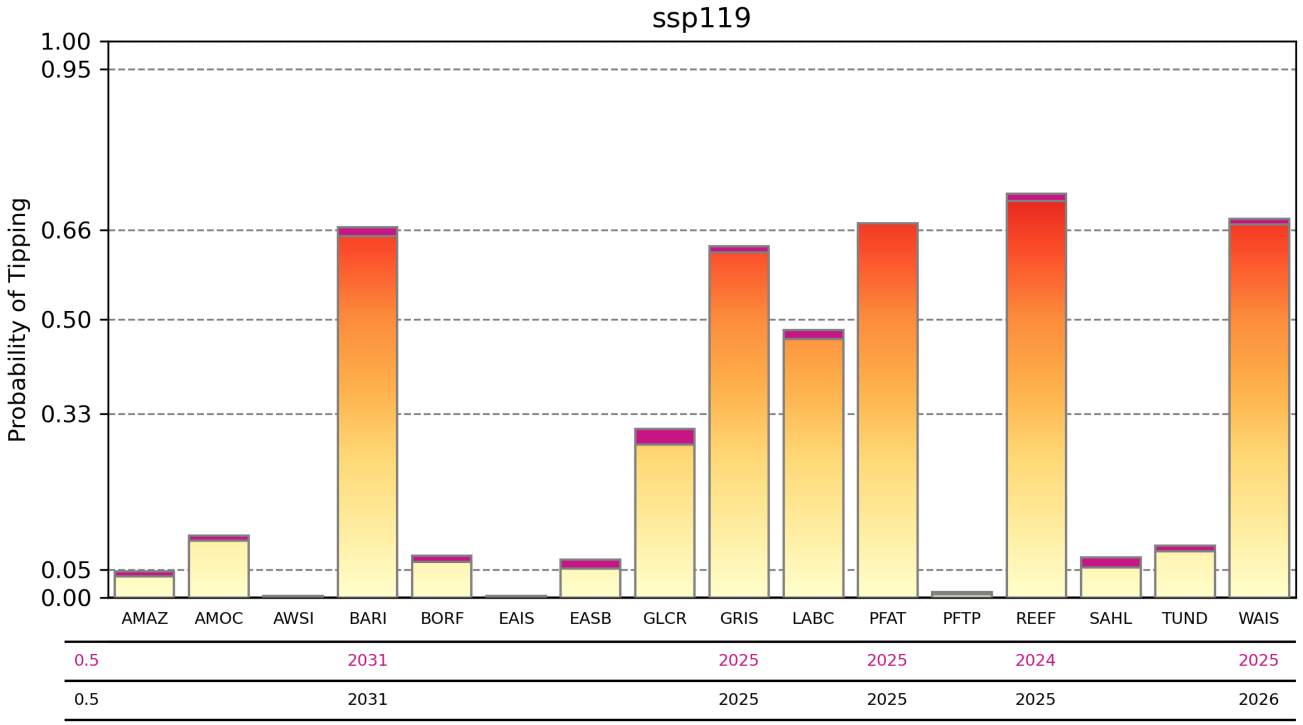


**Figure S12.** Probabilities of triggering the TEs by 2500 under SSP1-1.9. Additional probabilities from the carbon TEs are marked in purple. The table underneath states the years in which the 50% probability is crossed, with purple including carbon emissions from carbon TEs and black not.

## S10 Probabilities of Triggering Climate Tipping Elements in 2200

We also provide results for 2200 here to make our results comparable to the work of Kriegler et al. (2009),even though the increase in probabilities of triggering after 2200 is only 2% on average over all SSPs and TEs in the uncoupled ensemble.

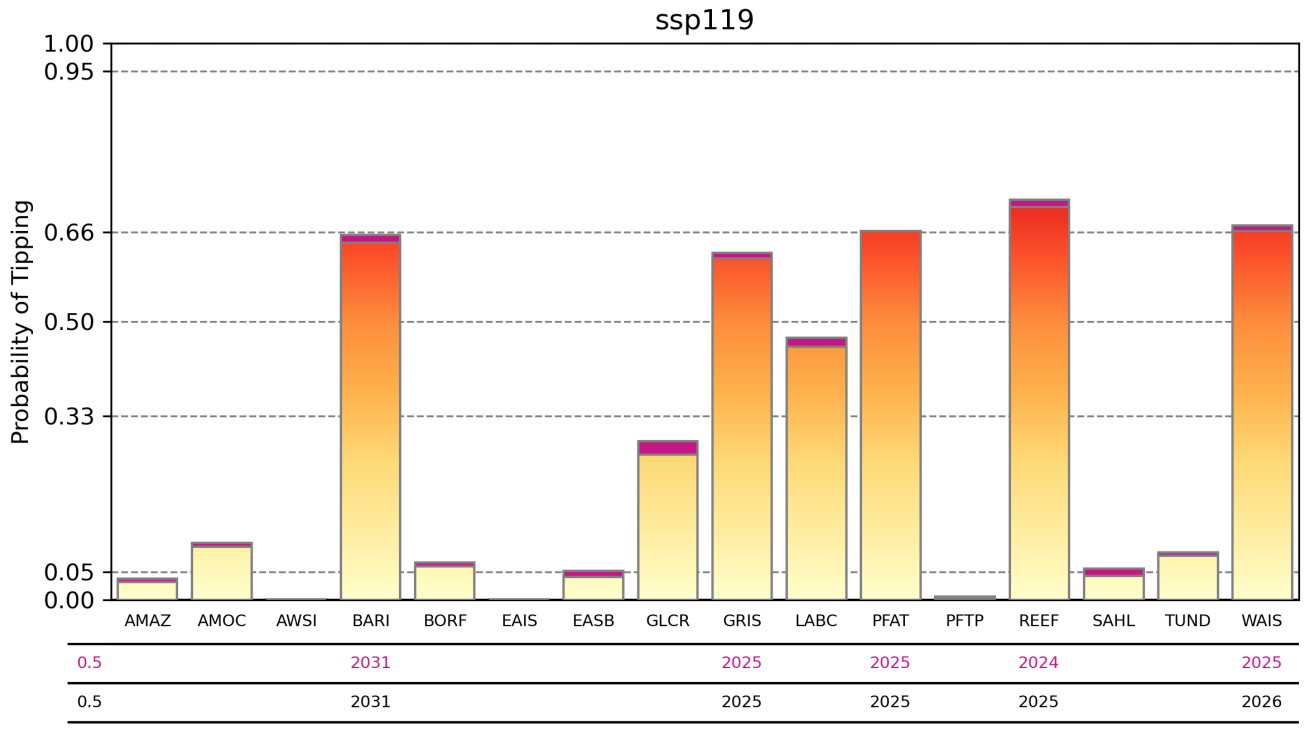


**Figure S13.** Probabilities of triggering the TEs by 2200 under SSP1-1.9. Additional probabilities from the carbon TEs are marked in purple. The table underneath states the years in which the 50% probability is crossed, with purple including carbon emissions from carbon TEs and black not.

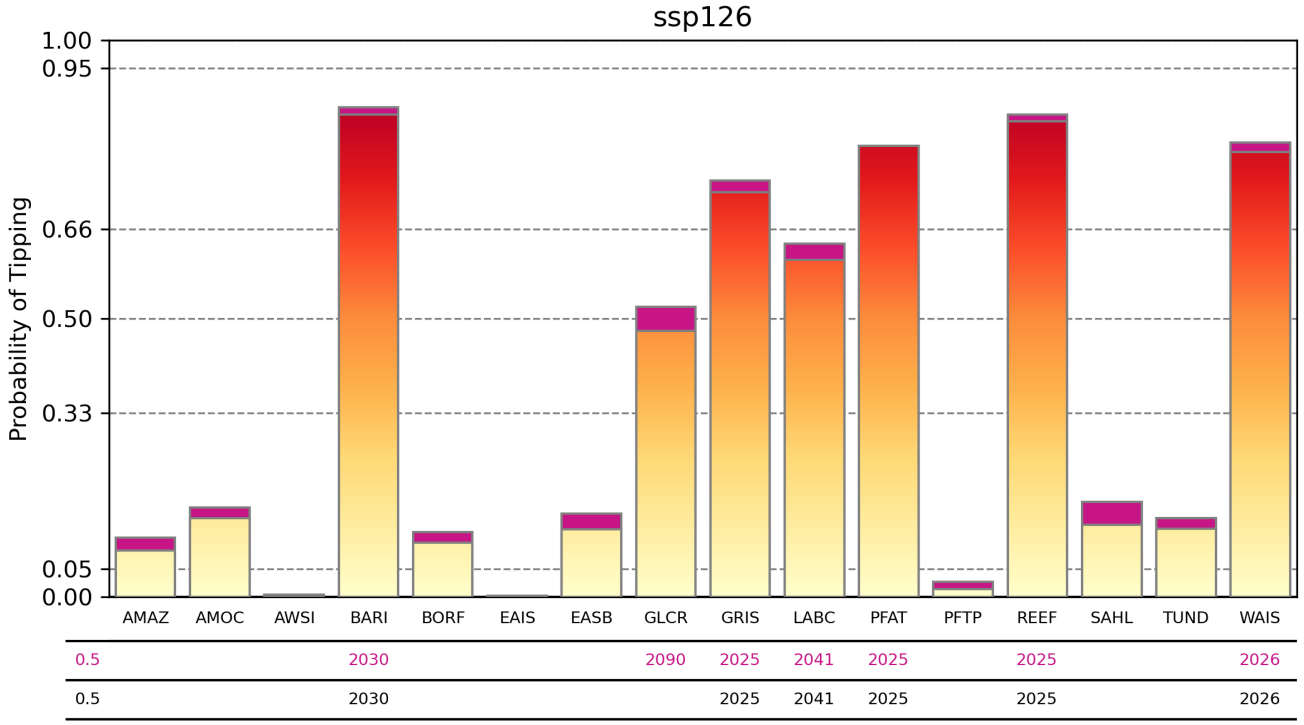


| | | | | | | | | | | | | | | | |
|---|---|---|---|---|---|---|---|---|---|---|---|---|---|---|---|
| 0.5 | | | 2030 | | | | 2090 | 2025 | 2041 | 2025 | | 2025 | | | 2026 |
| 0.5 | | | 2030 | | | | | 2025 | 2041 | 2025 | | 2025 | | | 2026 |

**Figure S14.** Probabilities of triggering the TEs by 2200 under SSP1-2.6. Additional probabilities from the carbon TEs are marked in purple. The table underneath states the years in which the 50% probability is crossed, with purple including carbon emissions from carbon TEs and black not.

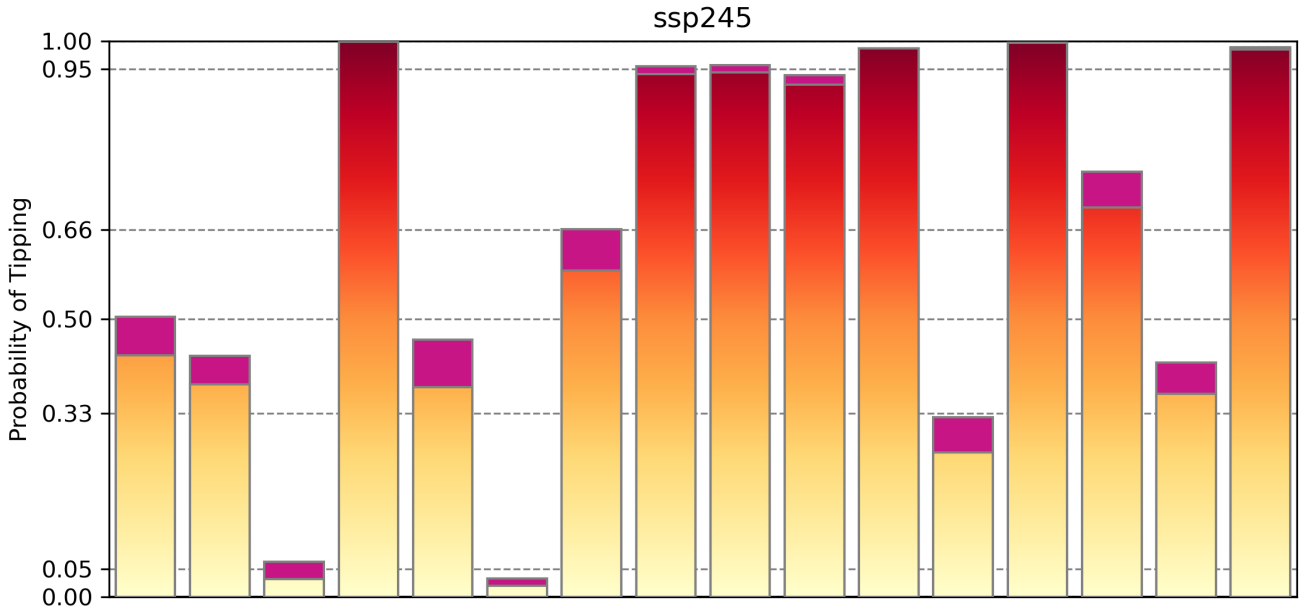


| | | | | | | | | | | | | | | | |
|---|---|---|---|---|---|---|---|---|---|---|---|---|---|---|---|
| 0.5 | 2196 | | 2029 | | | 2096 | 2046 | 2025 | 2037 | 2025 | | 2024 | 2080 | | 2025 |
| 0.5 | | | 2029 | | | 2122 | 2046 | 2025 | 2037 | 2025 | | 2024 | 2089 | | 2025 |
| 0.95 | | | 2047 | | | | 2158 | 2152 | | 2068 | | 2054 | | | 2069 |
| 0.95 | | | 2047 | | | | | | | 2068 | | 2055 | | | 2070 |

**Figure S15.** Probabilities of triggering the TEs by 2200 under SSP2-4.5. Additional probabilities from the carbon TEs are marked in purple. The table underneath states the years in which the 50% and the 95% probability are crossed, with purple including carbon emissions from carbon TEs and black not.

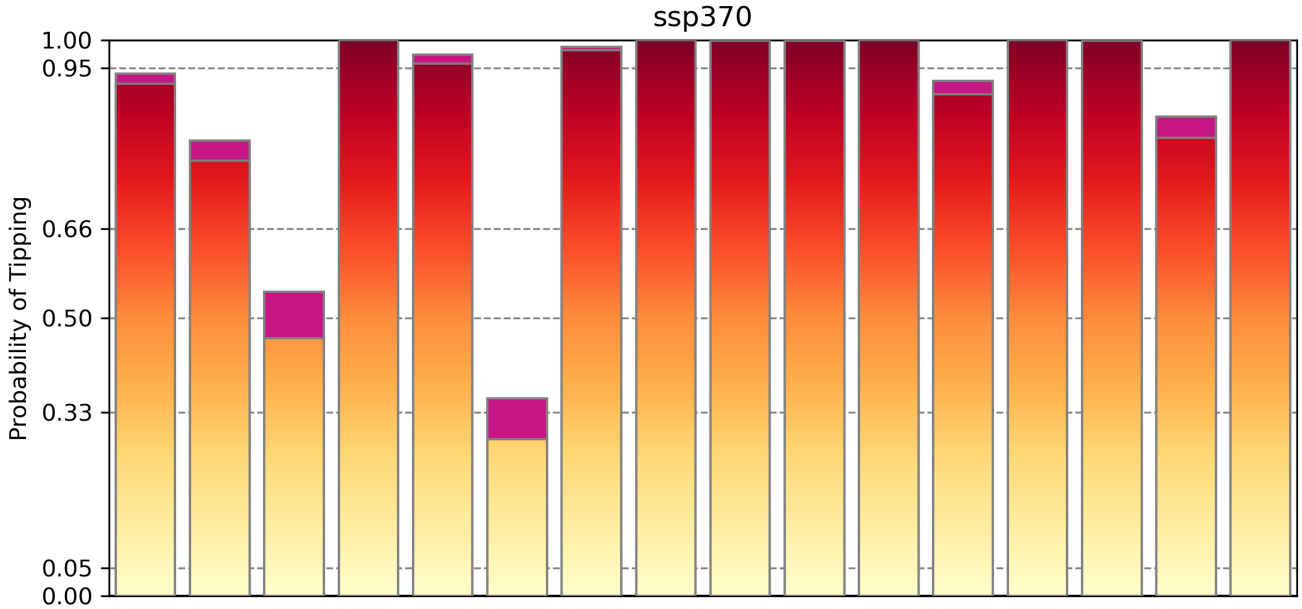


| | | | | | | | | | | | | | | | | |
|---|---|---|---|---|---|---|---|---|---|---|---|---|---|---|---|---|
| 0.5 | 2081 | 2092 | 2175 | 2029 | 2086 | | 2069 | 2042 | 2025 | 2035 | 2025 | 2095 | 2025 | 2064 | 2092 | 2025 |
| 0.5 | 2085 | 2098 | | 2029 | 2092 | | 2071 | 2043 | 2025 | 2035 | 2025 | 2100 | 2025 | 2065 | 2099 | 2025 |
| 0.95 | | | | 2042 | 2149 | | 2119 | 2070 | 2072 | 2079 | 2056 | | 2047 | 2095 | | 2055 |
| 0.95 | | | | 2042 | 2185 | | 2132 | 2071 | 2075 | 2082 | 2056 | | 2047 | 2099 | | 2056 |

**Figure S16.** Probabilities of triggering the TEs by 2200 under SSP3-7.0. Additional probabilities from the carbon TEs are marked in purple. The table underneath states the years in which the 50% and the 95% probability are crossed, with purple including carbon emissions from carbon TEs and black not.

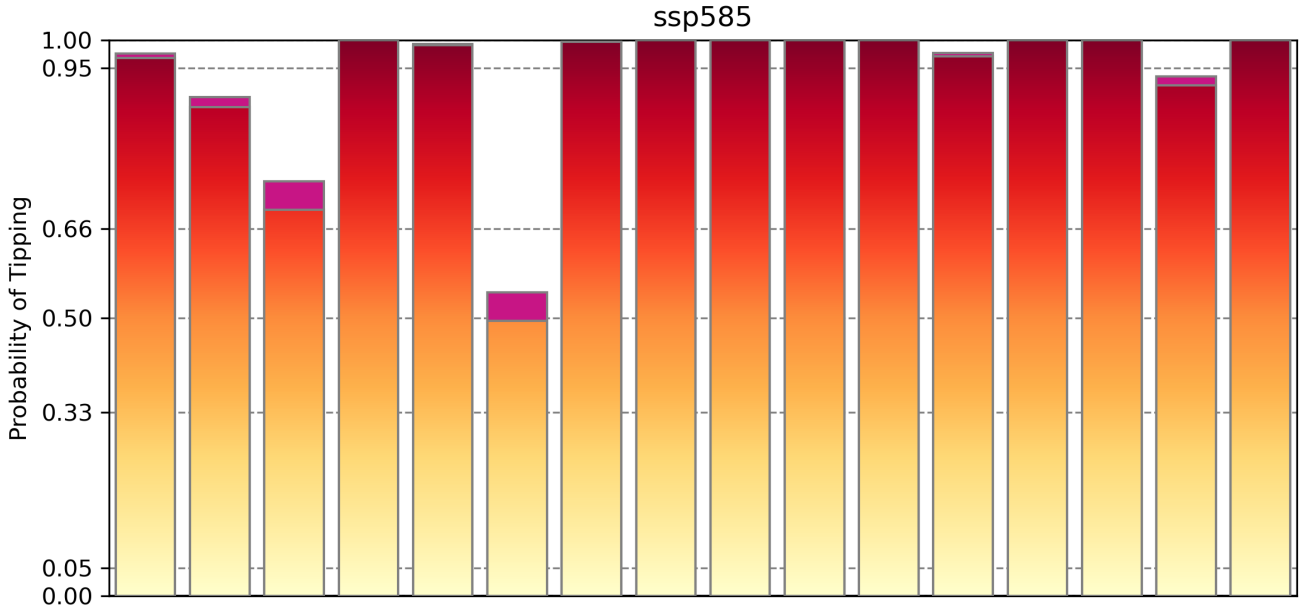


| | | | | | | | | | | | | | | | | |
|---|---|---|---|---|---|---|---|---|---|---|---|---|---|---|---|---|
| 0.5 | 2067 | 2075 | 2125 | 2026 | 2071 | 2178 | 2058 | 2037 | 2023 | 2031 | 2023 | 2078 | 2023 | 2053 | 2076 | 2023 |
| 0.5 | 2069 | 2079 | 2144 | 2026 | 2074 | | 2059 | 2037 | 2023 | 2031 | 2023 | 2081 | 2023 | 2054 | 2080 | 2023 |
| 0.95 | 2139 | | | 2037 | 2114 | | 2096 | 2059 | 2061 | 2066 | 2047 | 2145 | 2041 | 2079 | | 2048 |
| 0.95 | 2157 | | | 2038 | 2126 | | 2103 | 2059 | 2062 | 2067 | 2047 | 2163 | 2041 | 2081 | | 2048 |

**Figure S17.** Probabilities of triggering the TEs by 2200 under SSP5-8.5. Additional probabilities from the carbon TEs are marked in purple. The table underneath states the years in which the 50% and the 95% probability are crossed, with purple including carbon emissions from carbon TEs and black not.

## References


Armstrong McKay, D. I., Staal, A., Abrams, J. F., Winkelmann, R., Sakschewski, B., Loriani, S., Fetzer, I., Cornell, S. E., Rockström, J., and Lenton, T. M.: Exceeding 1.5°C global warming could trigger multiple climate tipping points, Science (New York, N.Y.), 377, eabn7950, https://doi.org/10.1126/science.abn7950, 2022.

Gao, F. and Han, L.: Implementing the Nelder-Mead simplex algorithm with adaptive parameters, Computational Optimization and Applications, 51, 259–277, https://doi.org/10.1007/s10589-010-9329-3, 2012.

Kriegler, E., Hall, J. W., Held, H., Dawson, R., and Schellnhuber, H. J.: Imprecise probability assessment of tipping points in the climate system, Proceedings of the National Academy of Sciences of the United States of America, 106, 5041–5046, https://doi.org/10.1073/pnas.0809117106, 2009.